01 Jun 2005

Hierarchical Optimal Force-Position-Contour Control of Machining Processes. Part II. Illustrative Example

Yan Tang

Robert G. Landers
Missouri University of Science and Technology, landersr@mst.edu

S. N. Balakrishnan
Missouri University of Science and Technology, bala@mst.edu

Recommended Citation

Y. Tang et al., "Hierarchical Optimal Force-Position-Contour Control of Machining Processes. Part II. Illustrative Example," *Proceedings of the American Control Conference (2005, Portland, OR)*, Institute of Electrical and Electronics Engineers (IEEE), Jun 2005.
The definitive version is available at https://doi.org/10.1109/ACC.2005.1470707

HIERARCHICAL OPTIMAL FORCE–POSITION–CONTOUR CONTROL OF MACHINING PROCESSES: PART II – ILLUSTRATIVE EXAMPLE

Yan Tang, Robert G. Landers, and S.N. Balakrishnan
Department of Mechanical and Aerospace Engineering
University of Missouri–Rolla
Rolla, Missouri 65409–0050
{ytnm4,landersr,bala}@umr.edu

ABSTRACT

There has been a tremendous amount of research in machine tool servomechanism control, contour control, and machining force control; however, to date these technologies have not been tightly integrated. This paper develops a hierarchical optimal control methodology for the simultaneous regulation of servomechanism positions, contour error, and machining forces. The contour error and machining force process reside in the top level of the hierarchy where the goals are to 1) drive the contour error to zero to maximize quality and 2) maintain a constant cutting force to maximize productivity. These goals are systematically propagated to the bottom level, via aggregation relationships between the top and bottom–level states, and combined with the bottom–level goals of tracking reference servomechanism positions. A single controller is designed at the bottom level, where the physical control signals reside, that simultaneously meets both the top and bottom–level goals. The hierarchical optimal control methodology is extended to account for variations in force process model parameters and process parameters. Simulations are conducted for four machining operations that validate the developed methodology. The results illustrate that the controller can simultaneously achieve both the top and bottom–level goals.

INTRODUCTION

There has been a tremendous amount of research in machine tool servomechanism control, contour control, and machining force control; however, to date these technologies have not been tightly integrated. These three areas have been researched separately in laboratory settings. However, there is no general methodology for combining these areas and, thus, integrating these technologies is a complex task. This paper will develop a hierarchical optimal control methodology that generates one controller that simultaneously regulates servomechanism positions, contour error, and machining forces.

In this paper, a hierarchical optimal control methodology is introduced that simultaneously regulates machining force processes, contour error, and servomechanism position errors in machining operations. The next section presents the control methodology and the following section extends the methodology to account for variations in force process model parameters and process parameters. Then, an example, namely, a two–axis turning operation, is presented and simulation studies for four operations are conducted to illustrate the utility of the hierarchical optimal control methodology.

ILLUSTRATIVE EXAMPLE: TWO–AXIS LATHE

The hierarchical optimal force–position–contour control methodology developed above is now applied to a two–axis lathe consisting of two linear orthogonal axes, denoted x and z, and a spindle. The x and z–axis time constants are denoted τ_x and τ_z, respectively, and the x and z–axis gains are denoted K_x and K_z, respectively. The control–oriented system equations of a two–axis servomechanism, assuming the electrical dynamic response is much faster than the mechanical dynamic response, are [Srinivassan and Tsao 1997]

$$\tau_x \ddot{x}_x(t) + \dot{x}_x(t) = K_x u_x(t) \tag{1}$$

$$\tau_z \ddot{x}_z(t) + \dot{x}_z(t) = K_z u_z(t) \tag{2}$$

The state space representation is

$$\boldsymbol{x}^T(t) = \begin{bmatrix} x_x(t) & x_z(t) & \dot{x}_x(t) & \dot{x}_z(t) \end{bmatrix} \tag{3}$$

$$\boldsymbol{u}^T(t) = \begin{bmatrix} u_x(t) & u_z(t) \end{bmatrix} \tag{4}$$

$$\boldsymbol{y}^T(t) = \begin{bmatrix} x_x(t) & x_z(t) \end{bmatrix} \tag{5}$$

$$A = \begin{bmatrix} 0 & 0 & 1 & 0 \\ 0 & 0 & 0 & 1 \\ 0 & 0 & -\frac{1}{\tau_x} & 0 \\ 0 & 0 & 0 & -\frac{1}{\tau_z} \end{bmatrix} \quad B = \begin{bmatrix} 0 & 0 \\ 0 & 0 \\ \frac{K_x}{\tau_x} & 0 \\ 0 & \frac{K_z}{\tau_z} \end{bmatrix} \quad G^T = \begin{bmatrix} 1 & 0 \\ 0 & 1 \\ 0 & 0 \\ 0 & 0 \end{bmatrix} \tag{6}$$

The augmented servomechanism system is

$$\dot{\boldsymbol{x}}_{\boldsymbol{bot}}(t) = \begin{bmatrix} E_{bot} & G_{bot} \\ 0_{(4)(4)} & A \end{bmatrix} \begin{bmatrix} \boldsymbol{e}(t) \\ \dot{\boldsymbol{e}}(t) \\ \boldsymbol{\xi}(t) \end{bmatrix} + \begin{bmatrix} 0_{(4)(2)} \\ B \end{bmatrix} \boldsymbol{u}_{\boldsymbol{bot}}(t) \tag{7}$$

where

$$\boldsymbol{e}^T(t) = \begin{bmatrix} e_x(t) & e_z(t) \end{bmatrix} \tag{8}$$

$$\boldsymbol{\xi}^T(t) = \begin{bmatrix} \ddot{x}_x(t) + \omega_r^2 x_x(t) & \ddot{x}_z(t) + \omega_r^2 x_z(t) \\ \ddot{x}_x(t) + \omega_r^2 \dot{x}_x(t) & \ddot{x}_z(t) + \omega_r^2 \dot{x}_z(t) \end{bmatrix} \tag{9}$$

$$E_{bot} = \begin{bmatrix} 0_{(2)(2)} & I_2 \\ -\omega_r^2 I_2 & 0_{(2)(2)} \end{bmatrix} \qquad G_{bot} = \begin{bmatrix} 0_{(2)(4)} \\ G \end{bmatrix} \tag{10}$$

$$\boldsymbol{u}_{bot}(t) = \begin{bmatrix} \ddot{u}_x(t) \\ \ddot{u}_z(t) \end{bmatrix} + \omega_r^2 \begin{bmatrix} u_x(t) \\ u_z(t) \end{bmatrix} \quad (11)$$

$$e_x(t) = x_x(t) - r_x(t) \quad (12)$$

$$e_z(t) = x_z(t) - r_z(t) \quad (13)$$

The vector $\boldsymbol{c}_1(t)$ is

$$\boldsymbol{c}_1(t) = \begin{bmatrix} c_x(t) & c_z(t) & 0_{(1)(6)} \end{bmatrix} \quad (14)$$

and c_x(t) and $c_z(t)$ depend upon the tool path. The change in feed is

$$\Delta f(t) = f_r(t) - f(t) = \frac{60\dot{r}_z(t)}{N_s} - \frac{60\dot{x}_z(t)}{N_s} = -\frac{60}{N_s}\dot{e}_z(t) \quad (15)$$

The spindle speed is assumed to be well regulated via another control scheme. The force error is

$$\Delta F(t) = -\frac{60\Theta(t)}{N_s}\dot{e}_z(t) \quad (16)$$

The aggregation matrix is

$$C(t) = \begin{bmatrix} c_x(t) & c_z(t) & 0 & 0 & 0_{(1)(4)} \\ 0 & 0 & 0 & -\frac{60\Theta(t)}{N_s} & 0_{(1)(4)} \end{bmatrix} \quad (17)$$

Applying the hierarchical optimal force–contour–position control methodology, the physical control signals are found by solving

$$\begin{bmatrix} \ddot{u}_x(t) \\ \ddot{u}_z(t) \end{bmatrix} + \omega_r^2 \begin{bmatrix} u_x(t) \\ u_z(t) \end{bmatrix} = -R_{bot}^{-1} B_{bot}^T P_{bot}(t) \boldsymbol{x}_{bot}(t) \quad (18)$$

SIMULATION STUDIES

Simulation studies are now conducted for the three turning operations shown in Figure 1. The servomechanism parameters are from a laboratory–grade machine tool [Landers, 1997]: $\tau_x = 0.055$ *sec*, $\tau_z = 0.056$ *sec*, $K_x = 3.628$ (*mm*/*s*)/*V*, and $K_z = 3.706$ (*mm*/*s*)/*V*. The force process is given by $F(t) = 1.17 f^{0.891}(t) d^{0.877}(t) V^{-0.273}(t)$. This data is based on machining experiments conducted for a steel part using a coated carbide insert [Sandoval *et al*., 2001]. The maximum power is 10 *hp* (7.46 *kW*) and the spindle speed is $N_s = 6000$ *rpm*. Interpolators, described below, generate the reference axis trajectories. A Runge–Kutta fourth order integration routine with a sample period of 0.001 *sec* is utilized to solve the servomechanism and controller dynamic equations. The control signals are saturated at ± 20 *V*. For all the simulations, the tool starts at rest at the *x*–*z* coordinate system origin. The *z*–axis reference velocity is

$$\dot{r}_z(t) = \frac{f_r(t) N_s}{60} \quad (19)$$

where the reference feed is calculated using the reference cutting force. The *x*–axis reference velocity is calculated from the *z*–axis reference velocity and the contour curvature. If the *x*–axis reference velocity is greater than the maximum *x*–axis velocity, the *x*–axis reference velocity is set to this maximum value and the *z*–axis reference velocity is recalculated. Six simulation case studies are investigated below. The three operations are shown in Figure 1. Each operation consists of a case study where the force process gain is constant and where the force process gain changes by 0.001 kN/mm^2 at each sample period. The weighting matrices, which were determined via trial and error, are $R_{bot} = diag\begin{bmatrix} 10^{-6} & 10^{-6} \end{bmatrix}$, $S_{bot} = 0$, $Q = diag\begin{bmatrix} 10^7 & 10^7 & 10^{-2} & 10^{-2} & 10^{-8} & 10^{-8} & 10^{-8} & 10^{-8} \end{bmatrix}$, and $Q_{bot} = diag\begin{bmatrix} 10^7 & 10^{-2} \end{bmatrix}$.

Operation I

The contour of Operation I (Figure 1a) comprises three sections. The first and third sections are straight lines with depths–of–cut of 2 *mm* and 1 *mm*, respectively and lengths–of–cut of 10 *mm*. The second section is a taper where the depth–of–cut continuously decreases from 2 *mm* to 1 *mm* over a length of 10 *mm*. The contour in each section has an infinite radius of curvature; thus, the reference angular velocity is zero at each section. The contour error in the first and third section is $e_x(t)$ and the contour error in the second section is

$$\varepsilon(t) = \frac{10}{\sqrt{1^2 + 10^2}} e_x(t) + \frac{1}{\sqrt{1^2 + 10^2}} e_z(t) \quad (20)$$

The simulation results for Cases 1 and 2 are shown in Figures 2 and 3, respectively. In Case 1, the force process gain is constant and the depth–of–cut varies during the second section. Therefore, the force–feed relation is given by equation (30) in Part I and the steady–state value of $P_{bot}(t)$ is calculated at each sample period. In Case 2, the force process gain varies and the depth–of–cut varies during the second section. Therefore, the force–feed relation is given by equation (26) in Part I and the steady–state value of $P_{bot}(t)$ is calculated at each sample period. The steady–state contour and force errors are zero in all three sections and for both cases since an exact contour error formulation was utilized and the feed was able to track the reference feed. There is slight contour error at the transitions between the straight and taper sections due to the discontinuity in the reference velocity at these points and control signal saturation.

Operation II

The contour of Operation II (Figure 1b) comprises three sections. The first and third sections are straight lines with depths–of–cut of 2 *mm* and 1 *mm*, respectively and lengths–of–cut of 5 *mm* and 10 *mm*, respectively. The second section is a quarter circle with a radius of 1 *mm*. The contours in the first and third sections have an infinite radius of curvature; thus, the reference angular velocity is zero in these sections. The reference angular velocity in the second section is the tangential reference velocity divided by the radius. The reference angular velocity will constantly vary in this section since the reference feed will vary due to the changing depth–of–cut. The exact contour error is [Koren and Lo, 1991]

$$\varepsilon(t)=\sqrt{\begin{matrix}\left\{\rho\sin\left[\phi(t)\right]+e_x(t)\right\}^2\\+\left\{\rho\cos\left[\phi(t)\right]+e_z(t)\right\}^2\end{matrix}}-\rho \tag{21}$$

where the radius of curvature is constant and is the circle radius. The time–varying, nonlinear aggregation relationship is approximated via a Taylor series expansion

$$\begin{aligned}\varepsilon(t)&=\left\{\sin\left[\phi(t)\right]+\frac{e_x(t)}{2\rho}\right\}e_x(t)\\&+\left\{\cos\left[\phi(t)\right]+\frac{e_z(t)}{2\rho}\right\}e_z(t)=c_x(t)e_x(t)+c_z(t)e_z(t)\end{aligned} \tag{22}$$

The simulation results for Cases 3 and 4 are shown in Figures 4 and 5, respectively. In Case 3, the force process gain is constant and the depth–of–cut varies during the second section. Therefore, the force–feed relation is given by equation (30) in Part I and the steady–state value of $P_{bot}(t)$ is calculated at each sample period. In Case 4, the force process gain and depth – of – cut vary during the second section. Therefore, the force–feed relation is given by equation (26) in Part I and the steady–state value of $P_{bot}(t)$ is calculated at each sample period. The steady–state contour and force errors are zero in the first and third sections and for both cases since an exact contour error formulation was utilized and the feed was able to track the reference feed. The contour error magnitude in the second section was less than 2 μm and the machining force error went towards zero. The non zero contour error was due to the approximation in equation (22). The tangent to the contour in this section changes from being solely in the z direction at the beginning of the contour to being solely in the x direction at the end of the contour. As a result, the reference z–axis velocity needed to maintain the machining force requires a x–axis reference velocity that exceeds its maximum value. Therefore, the x–axis reference velocity is set to its maximum value causing the reference z–axis velocity to decrease until it reaches zero at the end of the contour. This, in turn, causes the machining force to go towards zero. Again there is slight contour error at the transitions between the straight and circular sections due to the discontinuity in the reference velocity at these points and control signal saturation.

Operation III

The contour of Operation III (Figure 1c) comprises three sections. The first and third sections are straight lines with depths–of–cut of 2 *mm* and 1 *mm*, respectively and lengths–of–cut of 5 *mm* and 10 *mm*, respectively. The second section is a quarter ellipse with a major radius of a = 5 *mm* and a minor radius of b = 1 *mm*. The contours in first and third sections have an infinite radius of curvature; thus, the reference angular velocity is zero in these sections. The reference angular velocity in the second section is the tangential reference angular velocity divided by the instantaneous radius of curvature. The reference angular velocity will constantly vary in this section since the reference feed will vary due to the changing depth–of–cut. The x and z–axis reference positions, respectively, are

$$r_x(t)=X_c+b\sin\left[\phi(t)\right] \tag{23}$$

$$r_z(t)=Z_c+a\cos\left[\phi(t)\right] \tag{24}$$

The contour error is

$$\varepsilon(t)=\sqrt{\left[s_x(t)-X_{cc}(t)\right]^2+\left[s_z(t)-Z_{cc}(t)\right]^2}-\rho(t) \tag{25}$$

and the actual x and z–axis positions, respectively, are

$$s_x(t)=r_x(t)+e_x(t) \tag{26}$$

$$s_z(t)=r_z(t)+e_z(t) \tag{27}$$

The instantaneous radius of curvature and the coordinates of the instantaneous center of curvature, respectively, are

$$\rho(t)=\frac{\left(a^2\sin^2\left[\phi(t)\right]+b^2\cos^2\left[\phi(t)\right]\right)^{1.5}}{ab} \tag{28}$$

$$X_{cc}(t)=X_c+\frac{b^2-a^2}{b}\sin^3\left[\phi(t)\right] \tag{29}$$

$$Z_{cc}(t)=Z_c+\frac{a^2-b^2}{a}\cos^3\left[\phi(t)\right] \tag{30}$$

Substituting equations (26) and (27) into equation (25) and expanding the resulting equation by a second order Taylor's series expansion, the contour error is

$$\begin{aligned}\varepsilon(t)&=\left\{\frac{r_x(t)-X_{cc}(t)}{\rho(t)}+\frac{e_x(t)}{2\rho(t)}\right\}e_x(t)\\&+\left\{\frac{r_z(t)-Z_{cc}(t)}{\rho(t)}+\frac{e_z(t)}{2\rho(t)}\right\}e_z(t)=c_x(t)e_x(t)+c_z(t)e_z(t)\end{aligned} \tag{31}$$

The simulation results for Cases 5 and 6 are shown in Figures 6 and 7, respectively. In Case 5, the force process gain is constant and the depth–of–cut varies during the second section. Therefore, the force–feed relation is given by equation (30) in Part I and the steady–state value of $P_{bot}(t)$ is calculated at each sample period. In Case 6, the force process gain and depth – of – cut vary during the second section. Therefore, the force–feed relation is given by equation (26) in Part I and the steady–state value of $P_{bot}(t)$ is calculated at each sample period. The steady–state contour and force errors are zero in the first and third sections and for both cases since an exact contour error formulation was utilized and the feed was able to track the reference feed. The contour error magnitude in the second section was less than 4 μm and the machining force error went towards zero. The non zero contour error was due to the approximation in equation (31). The tangent to the contour in this section changes from being solely in the z direction at the beginning of the contour to being solely in the x direction at the end of the contour. As a result, the reference z–axis velocity needed to maintain the machining force requires a x–axis reference velocity that exceeds its maximum value. Therefore, the x–axis reference velocity is set to its maximum value causing the reference z–axis velocity to decrease until it reaches zero at the end of the contour. This, in turn, causes the machining force to go towards zero. Again there is slight contour error at the transitions between the straight and

elliptical sections due to the discontinuity in the reference velocity at these points and control signal saturation.

SUMMARY AND CONCLUSIONS

The hierarchical optimal control methodology developed in Part I was applied to a two–axis turning operation and simulations of three different operations were conducted to verify the developed methodology. Although the illustrative example was a two–axis turning operation, the methodology can be applied to most machining operations. The results showed that the controller is able to simultaneously achieve machining force, contour error, and servomechanism position error requirements. Thus, the proposed technique greatly decreases the complexity of the overall control system as separate machining force process and contour controllers are not required. The simulation results showed that the developed methodology could be applied to complex contours where machining force model parameters and process parameters were changing simultaneously. The hierarchical optimal control methodology presented in this paper provides a systematic strategy to integrate machining force process, contour, and servomechanism position control in machining operations.

NOMENCLATURE

A	nxn axis system state matrix
B	nxm axis system input matrix
C	aggregation matrix
$\boldsymbol{e}$	p–dimensional error vector [m]
$\dot{\boldsymbol{e}}$	p–dimensional error derivative vector [m/s]
e_x, e_z	x and z–axis position errors [m]
f	feed [mm]
f_r	reference feed [mm]
G	lxn axis system output matrix
I_j	identity matrix with j rows and j columns
K_x, K_z	x and z–axis velocity gains [(m/s)/V]
l	number of axis position measurements
N_s	spindle speed [rpm]
Q	bottom level weighting matrix
Q_{bot}	aggregation weighting matrix
r_x, r_z	x and z–axis reference positions [m]
$\dot{r}_x$, $\dot{r}_z$	x and z–axis reference velocities [m/s]
R_{bot}	dummy control signal weighting matrix
s_x, s_z	x and z–axis positions [m]
S_{bot}	final time aggregation weighting matrix
t	time [sec]
u_x, u_z	x and z–axis control inputs [V]
x_x, x_z	x and z–axis positions [m]
$\dot{x}_x$, $\dot{x}_z$	x and z–axis velocities [m/s]
$\ddot{x}_x$, $\ddot{x}_z$	x and z–axis accelerations [m/s^2]
$\dddot{x}_x$, $\dddot{x}_z$	x and z–axis jerks [m/s^3]
X_c, Z_c	x and z–contour centers [m]
X_{cc}, Z_{cc}	x and z–contour instantan. centers of curvature [m]
$\boldsymbol{y}$	l–dimensional axis measurement vector
ε	contour error [m]
ρ	contour instantaneous radius of curvature [m]
τ_x, τ_y	x and z–axis time constants [sec]
ϕ	contour polar angle [rad]
ω_r	contour reference angular velocity [rad/s]
$\boldsymbol{\xi}$	n–dimensional error space state vector
$0_{(i)(j)}$	zero matrix with i rows and j columns

REFERENCES

Koren Y. and Lo, C–C., 1991, "Variable Gain Cross Coupling Controller for Contouring," *Annals of the CIRP*, Vol. 40/1, pp. 371–374.

Landers, R.G., 1997, *Supervisory Machining Control: A Design Approach Plus Force Control and Chatter Analysis Components*, Ph.D. Dissertation, Department of Mechanical Engineering and Applied Mechanics, University of Michigan, Ann Arbor, Michigan.

Sandoval, J.E., Landers, R.G., and Ulsoy, A.G., 2001, "Reconfigurable CNC Lathe Simulation System," *ERC/RMS Technical Report*, University of Michigan, Ann Arbor, Michigan.

Srinivassan, K. and Tsao, T–C., 1997, "Machine Tool Feed Drives and Their Control – A Survey of the State of the Art," *ASME Journal of Manufacturing Science and Engineering*, Vol. 119, No. 4B, pp. 743–748.

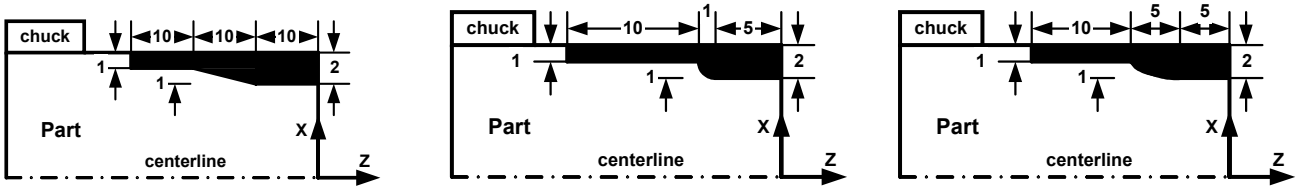

(a) Operation I **(b) Operation II** **(c) Operation III**

Figure 1: Four Lathering Operations – hatched area is material to be removed and all dimensions are in *mm*.

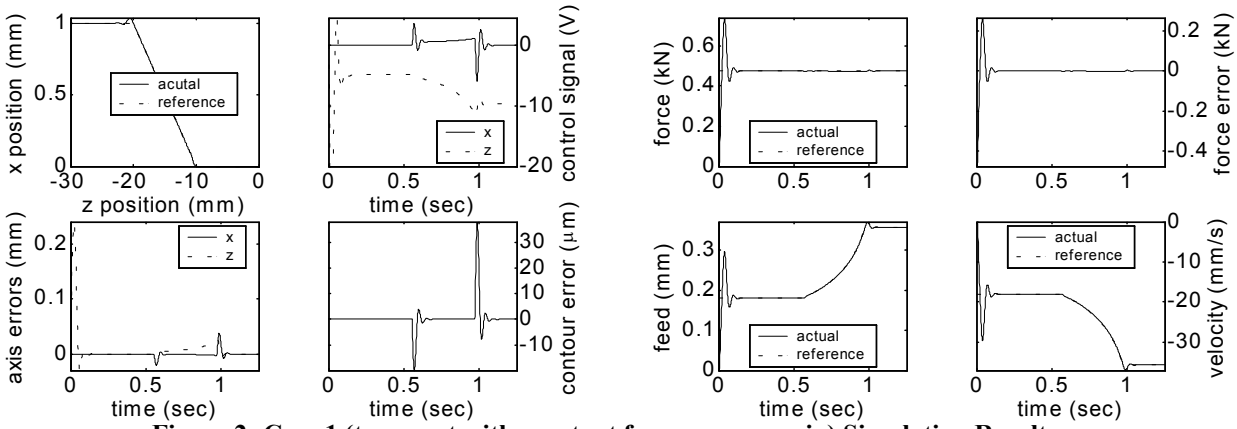

Figure 2: Case 1 (taper cut with constant force process gain) Simulation Results.

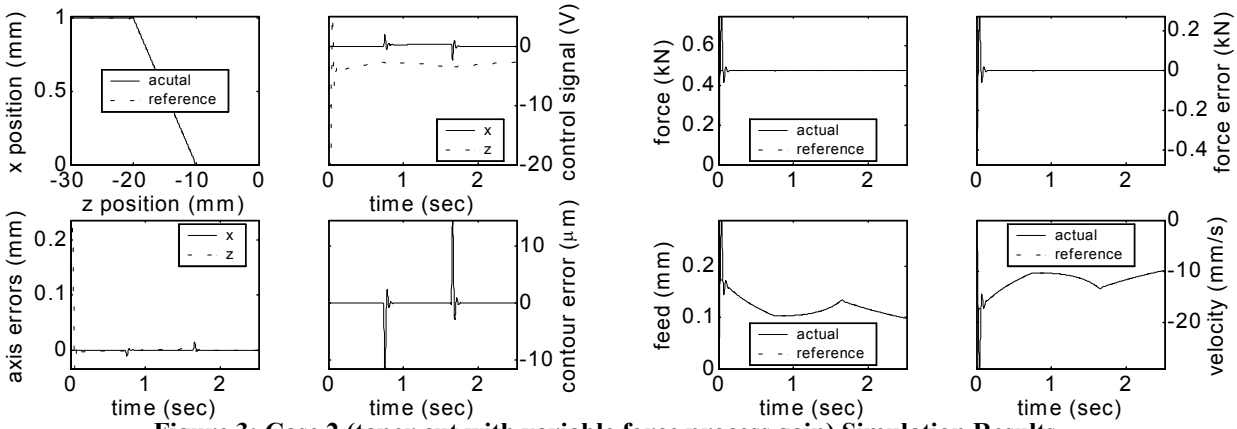

Figure 3: Case 2 (taper cut with variable force process gain) Simulation Results.

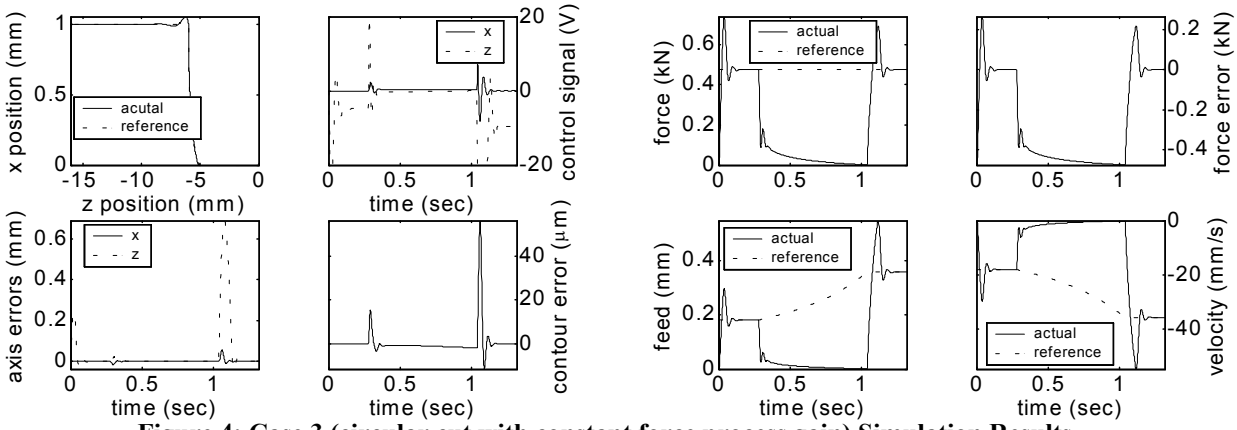

Figure 4: Case 3 (circular cut with constant force process gain) Simulation Results.

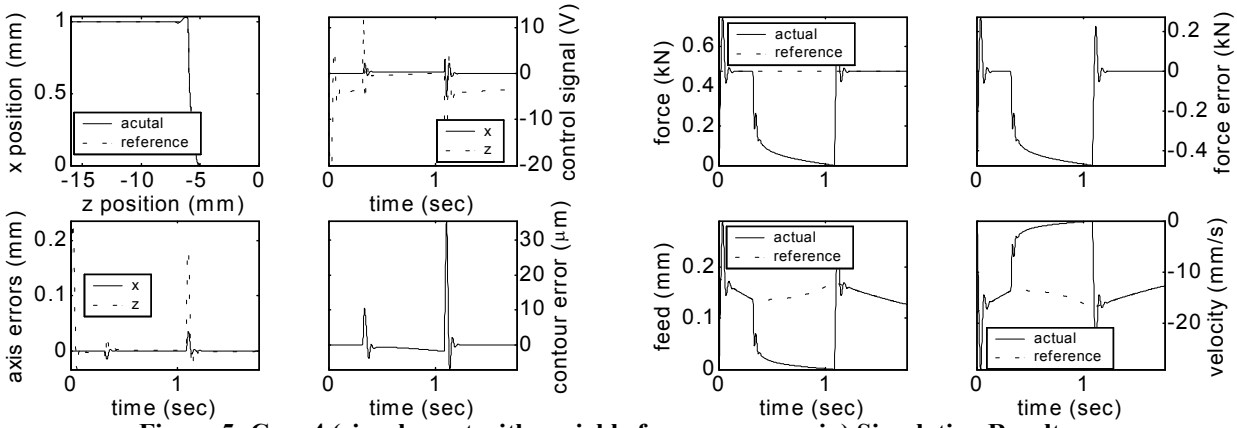

Figure 5: Case 4 (circular cut with variable force process gain) Simulation Results.

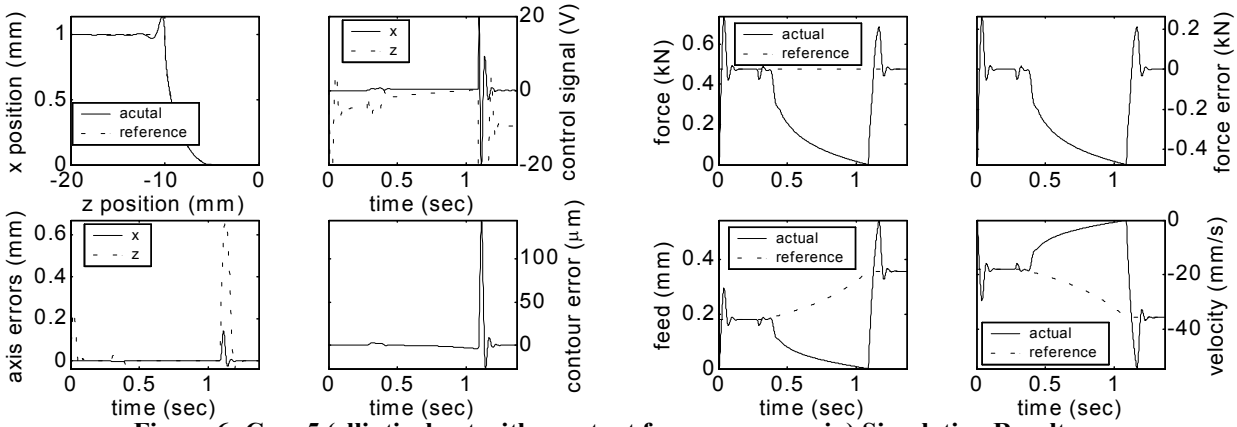

Figure 6: Case 5 (elliptical cut with constant force process gain) Simulation Results.

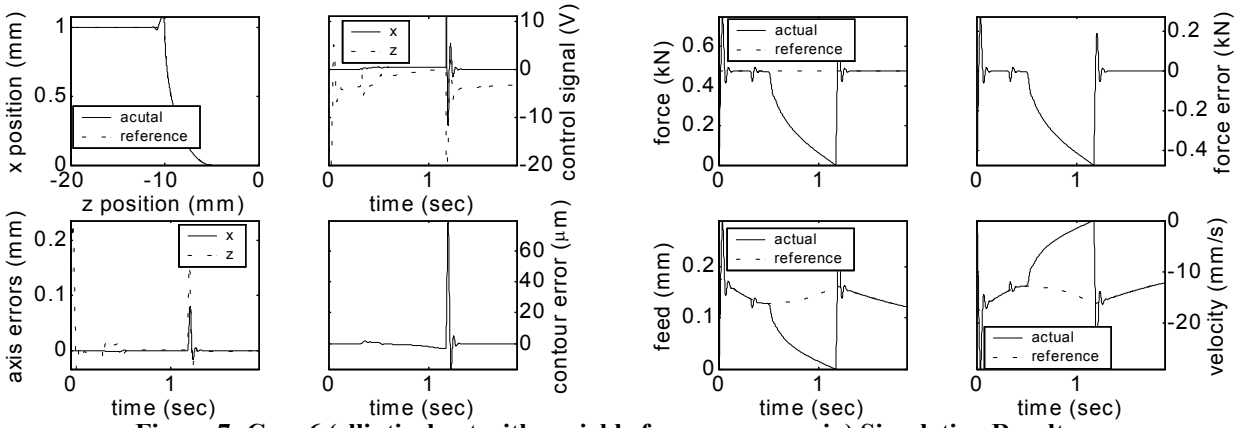

Figure 7: Case 6 (elliptical cut with variable force process gain) Simulation Results.